arXiv:0810.0020 [hep-ph], ANL-HEP-PR-08-59, NSF-KITP-08-46, SMU-HEP-08-16

Longitudinal Parity-violating Asymmetry in Hadronic Decays of Weak Bosons in Polarized Proton Collisions

Edmond L. Berger

High Energy Physics Division, Argonne National Laboratory, Argonne, Illinois 60439, USA

Pavel M. Nadolsky

Department of Physics, Southern Methodist University, Dallas, TX 75275, USA

(Dated: November 10, 2008)

Abstract

We investigate the possible measurement of parity-violating spin asymmetries in jet pair production in proton-proton collisions at the Brookhaven Relativistic Heavy Ion Collider (RHIC), with the goal to constrain longitudinally polarized quark and antiquark distribution functions. A measurable asymmetry could be observed in the vicinity of the massive weak W boson resonance, where the parity-violating signal appears above the parity-conserving background and is enhanced by interference of the strong and electroweak production amplitudes. We discuss the potential for such measurements, perhaps the first opportunity to measure a parity-violating asymmetry in proton-proton collisions at RHIC. Sensitivity of this measurement to the polarization of down-type antiquarks is demonstrated.

PACS numbers: 12.38.Bx, 13.87.-a, 13.88.+e

I. INTRODUCTION

The asymmetry in the rapidity-dependent cross section for weak (W) boson production in unpolarized high-energy $p\overline{p}$ collisions is a valuable instrument [1] for measuring the Bjorken x dependence of the ratio $u(x, M_W)/d(x, M_W)$ of the up-quark and down-quark quark parton distribution functions (PDFs) in a proton at the very hard scale set by the weak boson mass M_W. Demonstration of the utility of this prediction awaited sufficient luminosity [2, 3], but it was not long before the measured rapidity asymmetries were used routinely in global analyses as important constraints on unpolarized PDFs [4, 5]. The method relies on the accepted Drell-Yan mechanism by which the $W^{\pm}$ boson is produced in the standard model, e.g., principally $u + \bar{d} \to W^+$ and $d + \bar{u} \to W^-$ at leading order in quantum chromodynamics (QCD) perturbation theory. Thus, at least qualitatively, a W^+ moving with a large rapidity y is produced from projectile u quarks carrying large x, whereas a W^- moving with a large y is produced from projectile d quarks carrying large x. The ratio of the unpolarized W^+ and W^- cross sections at large y thus provides important constraints on the ratio $u(x, M_W)/d(x, M_W)$ at x between 0.1 and 1.

Extension of similar arguments to polarized pp scattering [6, 7, 8, 9, 10, 11] adds a promise of direct access to the longitudinal spin-dependent quark PDFs $\Delta q(x, M_W)$ via the $(V - A)$ coupling of the quark constituents to the W. Only one of the incident protons need be longitudinally polarized in order for this parity-violating measurement to be effective. In this paper we address W production in longitudinally polarized proton collisions at the Brookhaven Relativistic Heavy Ion Collider (RHIC) at collision energy $\sqrt{s} = 500$ GeV [12]. We focus on the dijet decay mode of the W, $pp \to (W \to jj) + X$, and compute fully differential cross sections in jet pair invariant mass Q, jet pair rapidity y, and jet transverse momentum p_{Tj} for all signal and background processes.

The parity-violating dijet production cross section, $\Delta\sigma = \sigma(p^{\rightarrow}p) - \sigma(p^{\leftarrow}p)$, where $p^{\rightarrow}$ ($p^{\leftarrow}$) represents a proton with its spin aligned with (against) the proton's direction of motion, is dominated by the $u\overline{d} + \overline{d}u \to W^+$ process. The single-spin asymmetry

$$A_L = \frac{\sigma(p^{\rightarrow}p) - \sigma(p^{\leftarrow}p)}{\sigma(p^{\rightarrow}p) + \sigma(p^{\leftarrow}p)}, \tag{1}$$

(as a function of the rapidity y) is sensitive to $\Delta u(x, M_W)$ at $x \to 1$ at large positive y values, and to $\Delta\overline{d}(x, M_W)$ at $x \to M_W^2/s$ at large negative y values, as we demonstrate quantitatively. Both Δu and $\Delta\overline{d}$ PDFs are not known well in the quoted x regions, as they are not constrained by the existing data (mostly from polarized deep inelastic scattering). The dijet asymmetry A_L may probe these PDFs with a relatively small event sample.

Commonly one detects a W boson by observing a leptonic decay $W \to \ell + \nu$, with its characteristic Jacobian peak in the transverse momentum p_T of the charged leptons $\ell = e$ or μ, and the missing transverse energy carried by the invisible neutrino ν.[1] The lepton decay mode is observable at all colliders, including RHIC [14, 15, 16]. Such signals are clean and impose tight constraints on the PDFs, but the small decay branching fraction penalty is felt keenly in the event rate. The luminosity in polarized proton scattering tends to be less than in the unpolarized case, and the W production cross section at the envisioned RHIC center-of-mass energy is not as great as at a higher-energy collider. Correspondingly,

[1] For a general discussion of production and observation of W bosons at hadron colliders, see, *e.g.,* Ref. [13].

lepton decay events come at a premium and most likely would require several years of RHIC running. With this in mind, it is attractive to investigate the *a priori* disfavored alternative that one could observe W production in the hadronic decay mode $W \to 2$ jets [17], precisely the topic of this paper.

An advantage of the hadronic W decay compared to the leptonic decay is a larger cross section, enhanced by $\mathrm{Br}(W \to \mathrm{hadrons})/\mathrm{Br}(W \to \ell\nu) \approx 6$. Another advantage is the possibility to directly determine the invariant mass and rapidity of the W boson, approximately equal in this case to the invariant mass (Q) and rapidity (y) of the high-p_T jet pair. The boson-level y distribution does not suffer from the smearing of the PDF dependence in the charged-lepton distributions [14] caused by spin correlations in the course of the W boson decay.

The hadronic decay mode of the W boson has an admitted drawback in that background contributions to jet pair production are substantial. Hadronic jets are produced most abundantly through QCD and electromagnetic (virtual photon) interactions, rather than through W interactions, especially via the scattering involving real gluons, which grows rapidly with collider energy. The backgrounds present a major obstacle for observing unpolarized electroweak (W and Z mediated) jet production at the Fermilab Tevatron $p\bar{p}$ collider and the CERN Large Hadron Collider [18, 19]. At the intermediate energy of RHIC, the background/signal ratio (25-30 or more) is comparable to that at the CERN $p\overline{p}$ Super Proton Synchrotron (SPS) with the energy $\sqrt{s} = 630$ GeV, where a 3σ enhancement from W and Z bosons in the dijet mass (Q) distribution was observed [20] with very low integrated luminosity ($\mathcal{L} = 0.73$ pb^{-1}).

We argue that the main backgrounds can potentially be controlled at RHIC because of their smooth (non-resonant) kinematical dependence and symmetry with respect to spatial reflections. Due to the smooth behavior, side-band subtraction can be used to advantage to estimate the *unpolarized* background accurately in the W signal region by extrapolation from the side bands of the Q distribution. The parity symmetry of the dominant background leads to its cancellation in the single-spin cross section, up to a small false asymmetry due to the uncertainty in the proton beam polarization. Thus the parity-violating A_L preserves the clear pattern of PDF flavor dependence typical of W boson production and allows us access to $\Delta u(x, M_W)$ and to $\Delta\overline{d}(x, M_W)$ in well-defined kinematic regions.

It is not possible to distinguish W^+ and W^- contributions in the jet pair decay mode. This apparent limitation does not disfavor the hadron decay mode with respect to the leptonic decay mode in situations in which charged lepton identification is not available, such as at the earlier stages of RHIC spin program. Full separation of the W and Z signals is not possible as a consequence of limited jet invariant mass resolution (of order 5-10 GeV). However, the Z contribution, with its relatively small event rate, has only mild effect on the PDF dependence of jet pair cross sections.

We evaluate all scattering processes for production of jet pairs (approximated by a pair of final-state partons) at the leading order in the QCD and electroweak coupling strengths, α_s and α_{EW}. Spin-dependent distributions in dijet mass (Q) and jet transverse momentum (p_{Tj}) at this order are reported in Ref. [17]. In our paper, we focus on fully differential distributions and comparison of dijet production channels, issues essential for the observation of A_L. We compute these distributions using a modified Monte-Carlo integrator MadEvent [21, 22, 23]. The presence of both strong and electroweak contributions to the same final state means that their constructive and destructive interference is possible. We compute the magnitude of the interference effect in both the unpolarized and the single-spin cross sections. Although

the interference effect enhances the single-spin cross section considerably, it does not alter the sensitivity of A_L to the polarized PDFs.

In a recent paper [24], Arnold *et al.* also consider jet production in polarized proton proton collisions at RHIC energies. Our focus and emphasis are somewhat different from theirs. In our work, we compute fully differential cross sections of two jets, whereas Ref. [24] investigates the single-jet inclusive double-differential cross section $d\sigma/(dp_{Tj}dy_j)$, integrated over the full range of dijet mass Q. All background contributions are included in the unpolarized denominator of A_L in Ref. [24], reducing predicted asymmetry values to about 1% or less. In our study, we find that selection cuts on Q and other kinematical variables, combined with the subtraction of the background in the signal region $70 < Q < 90$ GeV, are very effective in suppressing unpolarized dijet production. Owing to the use of these techniques our predictions for spin asymmetries are larger at least by an order of magnitude, and our appraisal of the jet pair mode is more optimistic.

A tag on final-state charmed hadrons is proposed in Ref. [24] as a means to improve the signal over the background. In principle charm tagging eliminates the dominant gluon and light-quark parity-conserving processes, while preserving a large fraction [of order $\mathrm{Br}\,(W \to cX)\,/\mathrm{Br}\,(W \to \mathrm{all}) \approx 33\%$] of electroweak signal events. In practice, the utility of this approach is diminished by the low efficiency of the experimental identification of final-state charmed hadrons. Charm scattering contributions are included in our Monte-Carlo calculation, so that charm tagging can be explored together with the other handles at the fully differential level.

In Sec. II, we discuss the basic QCD processes that produce a pair of jets. We show figures that illustrate the size of various QCD and electroweak contributions to the cross section, as a function of the dijet invariant mass and other variables. To obtain our quantitative estimates of polarization asymmetries in Sec. III, we must adopt parametrizations of spin dependent parton distributions. We choose to work with the de Florian-Navarro-Sassot parametrization [25]. Using these PDFs, we explore sensitivity of the predictions for A_L to variations in the spin-dependent PDF parametrizations.

Conclusions are summarized in Sec. IV. Our quantitative predictions show that the predicted magnitude of A_L is sufficiently large relative to the anticipated uncertainties, so that significant measurements should be possible, with good prospects for discrimination among different polarized PDFs. We urge experimental study of $A_L(y)$ in hadronic decays of W at RHIC.

II. UNPOLARIZED JET PAIR PRODUCTION

A. General remarks

We consider inclusive jet pair production in proton-proton collisions at $\sqrt{s} = 500$ GeV, $pp \to jjX$, approximated by $2 \to 2$ exchanges of the standard model bosons ($V = g$, γ^*, $W^\pm$, and Z^0) in the s, t, and u channels, including the interference between the amplitudes with different types of the bosons. The unpolarized and single-spin cross sections, σ and $\Delta\sigma$, for production of an energetic jet pair are given by

$$\frac{d\sigma}{d\vec{p}_1 d\vec{p}_2} = \sum_{a,b,c,d} \frac{d\widehat{\sigma}(ab \to cd)}{d\vec{p}_1 d\vec{p}_2} f_{a/p}(x_1, Q) f_{b/p}(x_2, Q), \tag{2}$$

and

$$\frac{d\Delta\sigma}{d\vec{p}_1 d\vec{p}_2} = \sum_{a,b,c,d} \frac{d\Delta\widehat{\sigma}(ab \to cd)}{d\vec{p}_1 d\vec{p}_2} \Delta f_{a/p}(x_1, Q) f_{b/p}(x_2, Q), \tag{3}$$

where p_1^μ and p_2^μ are the momenta of the jets, $Q^2 = (p_1 + p_2)^2$, $x_{1,2} = Qe^{\pm y}/\sqrt{s}$, $y = \ln\left[\left(Q^0 + Q^3\right)/\left(Q^0 - Q^3\right)\right]/2$, $(\Delta)\widehat{\sigma}(ab \to cd)$ is the perturbative cross section in the $ab \to cd$ parton scattering channel, and $f_{a/p}(x, Q)$ ($\Delta f_{a/p}(x, Q)$) is the unpolarized (longitudinally polarized) PDF. The QCD renormalization and factorization scales are set equal to the invariant mass Q of the dijet. The z axis follows the direction of the polarized proton beam. In some cases, we use the notation $\sigma(V)$ for the partial cross section that involves the same boson species V in the scattering amplitude and its conjugate, without the interference with other types of bosons.

The lowest-order cross sections for s-channel W^+ (W^-) production via $q_i\overline{q}_j \to W^\pm \to q_k\overline{q}_l$ (the dominant parity-violating contribution) are

$$\frac{d\sigma(W,\, s\text{-channel})}{dQ^2 dy} = \sum_{i,j} C_{ij} \left[q_i(x_1, Q)\overline{q}_j(x_2, Q) + \overline{q}_j(x_1, Q) q_i(x_2, Q)\right] \tag{4}$$

and

$$\frac{d\Delta\sigma(W,\, s\text{-channel})}{dQ^2 dy} = \sum_{i,j} C_{ij} \left[-\Delta q_i(x_1, Q)\overline{q}_j(x_2, Q) + \Delta\overline{q}_j(x_1, Q)\overline{q}_i(x_2, Q)\right], \tag{5}$$

where

$$C_{ij} = \frac{\pi^2 \alpha_{EW}^2}{12s} \frac{Q^2}{\left(Q^2 - M_W^2\right)^2 + \Gamma_W^2 Q^4/M_W^2} \left|V_{ij}\right|^2 \sum_{k,l} \left|V_{kl}\right|^2,$$

$\alpha_{EW} = g_w^2/4\pi$ is the electroweak coupling strength, M_W and Γ_W are the W boson mass and width, and $V_{ij} = V_{ji}$ is the quark mixing (Cabibbo-Kobayshi-Maskawa) matrix. The indices i, j, k, l are summed over flavors of quark-antiquark pairs carrying the net electric charge of the W^+ or W^- boson. At the energy of RHIC, where contributions with initial-state s, c, b (anti-)quarks are much smaller than those with u and d (anti-)quarks, the W^+ and W^- cross sections are well approximated by

$$\frac{d\sigma(W^+,\, s\text{-channel})}{dQ^2 dy} = C_{ud} \left[u(x_1, Q)\bar{d}(x_2, Q) + \bar{d}(x_1, Q) u(x_2, Q)\right] + \text{ small terms}; \tag{6}$$

$$\frac{d\sigma(W^-,\, s\text{-channel})}{dQ^2 dy} = C_{ud} \left[d(x_1, Q)\bar{u}(x_2, Q) + \bar{u}(x_1, Q) d(x_2, Q)\right] + \text{ small terms}; \tag{7}$$

$$\frac{d\Delta\sigma(W^+,\, s\text{-channel})}{dQ^2 dy} = C_{ud} \left[-\Delta u(x_1, Q)\bar{d}(x_2, Q) + \Delta\bar{d}(x_1, Q) u(x_2, Q)\right] + \text{ small terms}; \tag{8}$$

and

$$\frac{d\Delta\sigma(W^-,\, s\text{-channel})}{dQ^2 dy} = C_{ud} \left[-\Delta d(x_1, Q)\bar{u}(x_2, Q) + \Delta\bar{u}(x_1, Q) d(x_2, Q)\right] + \text{ small terms}. \tag{9}$$

These resonant cross sections are combined with non-resonant ($t-$ and u-channel) contributions to form $\sigma(W)$, the full W-boson contribution of order α_{EW}^2. In a similar manner, we construct pure Z and γ^* contributions, also of order α_{EW}^2. In addition, one must include

the cross section for the interference between the electroweak bosons (of order α_{EW}^2), and between the electroweak bosons and gluons (of order $\alpha_S \alpha_{EW}$). Finally, there is a pure QCD cross section, of order α_s^2. Explicit matrix elements for all these processes can be found in Ref. [17].

Our fully differential spin-dependent cross sections for $2 \to 2$ jet production are computed in all channels with the help of the programs MadGraph and MadEvent [21, 22, 23]. MadGraph is a program for automatic generation of tree-level cross sections in the standard model and its common extensions. MadEvent realizes phase-space integration of these cross sections. Internally these programs operate with helicity-dependent scattering amplitudes obtained using the HELAS library [26]. In a typical setting, the amplitudes are summed over all helicity combinations to produce spin-averaged cross sections. We modified MadEvent to also allow evaluation of single-spin cross sections for an arbitrary scattering process, including jet pair production.[2] This modified program is employed to evaluate both the numerator and denominator of A_L.

In hard-scattering cross sections, we include contributions from four quark flavors (u, d, s, and c), in accordance with the default MadGraph choice. The unpolarized and longitudinally polarized PDFs are taken from the Martin-Roberts-Stirling-Thorne (MRST'2002 NLO [27]) and de Florian-Navarro-Sassot (DNS'2005 [25]) sets, respectively. The MRST'2002 NLO PDFs are chosen because they satisfy positivity conditions with the DNS'2005 PDFs.

B. Kinematic distributions of unpolarized cross sections

Spin-averaged jet production is dominated by the continuous event distribution from QCD and electromagnetic scattering (involving only g and γ^*). These involve, in order of their magnitudes at $60 < Q < 100$ GeV, $qg \to qg$, $gg \to gg$, $qq' \to qq'$, $qq \to qq$, and smaller scattering contributions, where q stands for both quarks and antiquarks, and qq (qq') stands for scattering of the same (different) quark flavors. The two largest jet cross sections produced by qg and gg scattering cancel when a cross section difference is taken to compute the single-spin asymmetry. Parity violation needed to obtain a non-zero numerator of A_L in Eq. (1) arises solely from qq contributions with intermediate W and Z bosons. The s-channel parity-violating scattering amplitudes are enhanced resonantly when the dijet invariant mass Q is close to M_W (M_Z), in the Q range we will call "the signal region". Even in this region, the spin-averaged W and Z contribution constitutes at most a few percent of the full event rate, suggesting that the most straightforward measurement (not separating the signal and background contributions) would result in small spin asymmetries. The magnitude of A_L may be enhanced by applying a "side-band subtraction" technique, i.e., by measuring the large parity-conserving background at values of Q outside of the signal region and subtracting it from the denominator of A_L inside the signal region.

Let us now turn to the figures illustrating these observations. The spin-averaged differential cross sections for various combinations of scattering channels are shown in Fig. 1. We focus on the distributions in the dijet invariant mass Q, the transverse momentum p_{Tj} of the jet, and the difference Δy of jet rapidities, $\Delta y = |y_1 - y_2|$, shown in Figs. 1(a,b,c). Cross sections denoted "$W(\alpha_{EW}^2)$", "$Z(\alpha_{EW}^2)$", and "$\gamma^*(\alpha_{EW}^2)$" represent the pure W boson contri-

[2] The modified MadEvent program for the calculation of polarized cross sections is available from one of the authors (P.M.N.) by request.

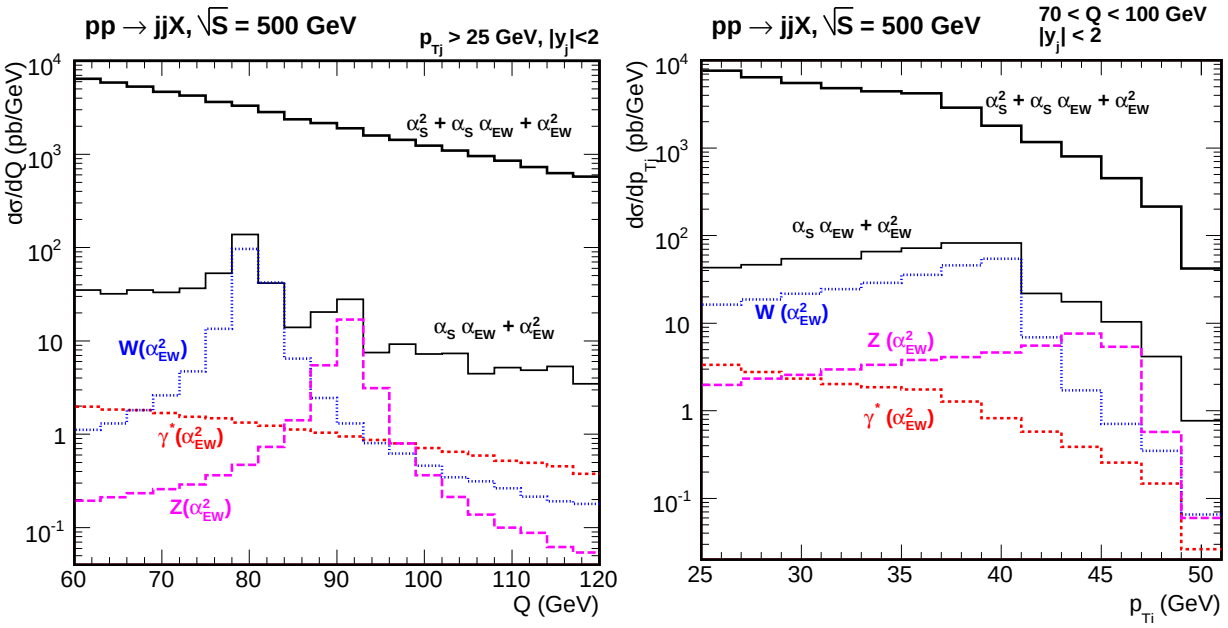

(a) (b)

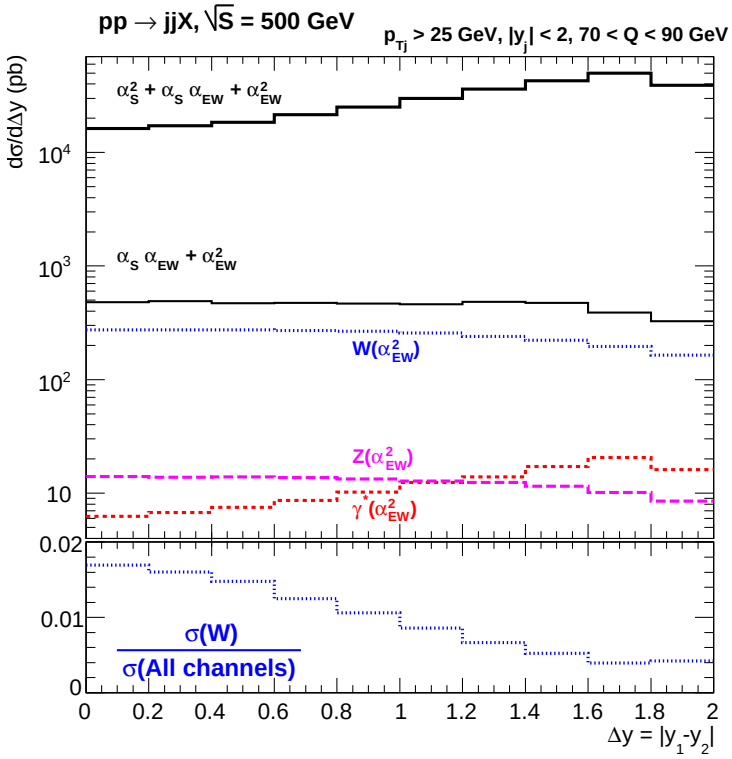

(c)

Figure 1: Unpolarized cross sections for $pp \to jjX$ at $\sqrt{s} = 500$ GeV in various scattering channels, plotted as a function of (a) dijet invariant mass Q, (b) jet transverse momentum p_{Tj}, and (c) difference of jet rapidities $\Delta y = |y_1 - y_2|$, for the cuts specified in the figures.

bution, the Z boson contribution, and the γ^* contribution, without the interference terms. The sum of all electroweak and interference cross sections is shown by a lower solid line labeled "$\alpha_s\alpha_{EW}+\alpha_{EW}^2$". The full cross section, which also includes the pure QCD contribution of order α_s^2, is shown by the upper solid line with the label "$\alpha_S^2+\alpha_s\alpha_{EW}+\alpha_{EW}^2$".

In most figures, we impose constraints $p_{Tj} > 25$ GeV and $|y_j| < 2$ to reproduce approximately the acceptance of the STAR detector [28].[3] As seen in Figs. 1(a) and (b), W (Z) production receives a resonant enhancement at $Q \approx M_W$ (M_Z) and $p_{Tj} \approx M_W/2$ ($M_Z/2$). The QCD and electromagnetic backgrounds fall smoothly with both Q and p_{Tj}. To focus on the parity-violating asymmetry, we impose a selection $70 < Q < Q_{max}$, with $Q_{max} = 90-100$ GeV, in Figs. 1(b) and (c). A value of Q_{max} below M_Z is generally preferred in order to suppress the Z cross section (constituting about 1/6 of $\sigma(W)$ at their respective mass poles according to Fig. 1(a)) and emphasize the PDF dependence typical for the W boson contribution.

In $2 \to 2$ scattering, Δy is related to the scattering angle θ_* in the jet pair rest frame as $\tanh(\Delta y/2) = \cos\theta_*$. Signal and background processes are characterized by different spin correlations between the initial- and final-state particles and, therefore, different shapes of $d\sigma/d(\cos\theta_*)$ [or $d\sigma/d\Delta y$]. The kinematic differences between the signal and background $d\sigma/d\Delta y$ distributions are traced largely to real-gluon emissions present in the QCD background process, but not in the electroweak processes (see below). Figure 1(c) shows that the full $\mathcal{O}(\alpha_S^2+\alpha_s\alpha_{EW}+\alpha_{EW}^2)$ cross section is peaked strongly at large $|\Delta y|$, while the signal $\mathcal{O}(\alpha_{EW}^2)$ and $\mathcal{O}(\alpha_{EW}^2+\alpha_s\alpha_{EW})$ cross sections have flatter $|\Delta y|$ dependence.In the dijet rest frame, the $\mathcal{O}(\alpha_S^2+\alpha_s\alpha_{EW}+\alpha_{EW}^2)$ cross section peaks more strongly at $\cos\theta_* \to \pm 1$ as compared to the $\mathcal{O}(\alpha_{EW}^2+\alpha_s\alpha_{EW})$ cross section.

The full electroweak+interference cross section constitutes 2-3% of the full cross section at $|\Delta y| = 0$, but it drops below 1% at $|\Delta y| \approx 2$. This difference could be exploited to enhance the signal/background ratio. For simplicity, we don't impose this selection in the rest of the paper.

In Fig. 2 we examine the flavor composition and angular dependence of QCD scattering channels (proportional to α_s^2). In the relevant region of Q, QCD jet production is dominated by quark-gluon scattering, $qg \to qg$, and, at lower Q values (not shown) by gluon-gluon scattering $gg \to gg$ (cf. Fig. 2(a)). Both types of contributions are peaked strongly at large $|\Delta y|$; see Fig. 2(b). The quark-quark scattering QCD contributions, $qq \to qq$ and $qq' \to qq'$, have a flatter dependence on Q and $|\Delta y|$ than the gluon-scattering contributions. Similarly, the electroweak $\mathcal{O}(\alpha_{EW}^2+\alpha_s\alpha_{EW})$ dijet production, also proceeding via quark-quark scattering, has a flatter dependence on $|\Delta y|$ than the gluon-scattering-dominated QCD background.

The $qq \to qq$ and $qq' \to qq'$ QCD amplitudes can interfere with the electroweak amplitudes having the same initial and final quark states. The largest contributions to the interference, together with the full interference term, are shown in Fig. 3 as a function of Q. The magnitude of the $\mathcal{O}(\alpha_s\alpha_{EW})$ interference is similar to that of the $\mathcal{O}(\alpha_{EW}^2)$ cross section. Its shape is determined by the interplay of the partial interference terms.

We classify these partial terms according to their initial-state quark composition. That is, the cross section "uu, dd" corresponds to the sum of the interference cross sections with two initial-state u quarks or two d quarks, i.e., $uu \to uu$ and $dd \to dd$; "ud" corresponds

[3] Our results for an asymmetric cut $-2 \le y_j \le 1$ on jet rapidities (exactly corresponding to the STAR acceptance) are qualitatively similar.

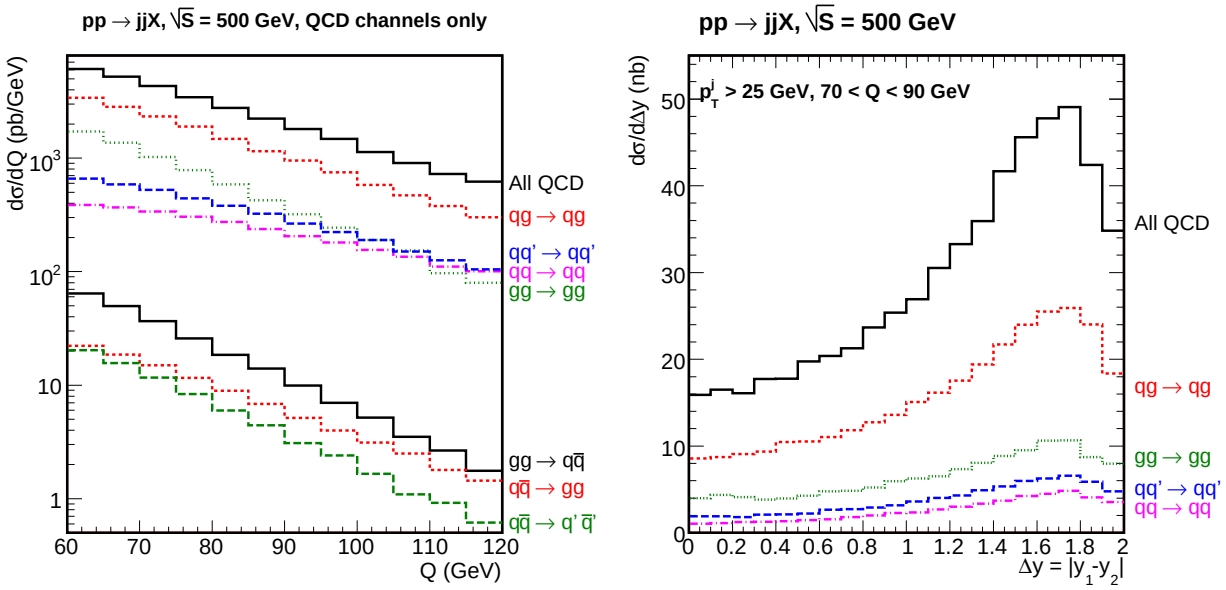

(a) (b)

Figure 2: $\mathcal{O}(\alpha_s^2)$ cross sections for $pp \to jjX$ at $\sqrt{s} = 500$ GeV in various scattering channels (QCD contributions only), plotted versus (a) dijet invariant mass Q, (b) difference of jet rapidities $\Delta y = |y_1 - y_2|$.

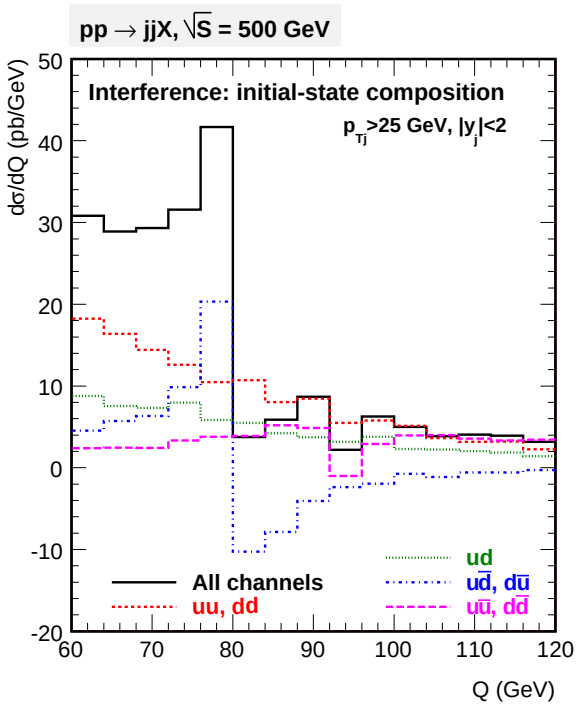

Figure 3: The unpolarized interference cross section (solid) and contributions of individual initial-state channels: uu and dd (short-dashed); ud (dotted); $u\bar{d}$ and $d\bar{u}$ (dot-dashed); $u\bar{u}$ and $d\bar{d}$ (long-dashed).

to the interference cross section for $ud \to ud$, $ud \to du$, $du \to ud$, and $du \to du$; and so on. Smaller interference terms involving strange or charm quarks are included in the total interference, but not shown separately.

It is useful to distinguish between the interference terms that possess resonant properties and those that do not. The resonant interference occurs between an s-channel W or Z boson amplitude and a different conjugate amplitude with the same external states. The real part of the heavy boson propagator in the s-channel amplitude changes sign at the boson's mass pole, $Q = M_V$. Consequently a resonant interference term exhibits a pronounced enhancement slightly below the W or Z pole and a comparable enhancement of the opposite sign immediately above the pole. In our case, the "$u\bar{d}$, $d\bar{u}$" cross section (dot-dashed curve) is the most prominent resonant term dominated by the interference with the $s-$channel W boson amplitude. It changes sign at $Q = M_W$. Despite its large magnitude, its contribution to the integrated event rate in the signal region $70 < Q < 90$ GeV is small, due to the cancellation between the contributions of the opposite sign from below and above $Q = M_W$. Similarly, a resonance driven by the s-channel Z boson amplitude occurs in the "$u\bar{u}$, $d\bar{d}$" cross section (long-dashed line) at $Q = M_Z$.

The largest interference contributions to the integrated rate in the signal region arise from non-resonant uu, ud, and dd processes (short-dashed and dotted lines). These cross sections do not contain a large resonant propagator, but rather are enhanced by a product of two large valence-dominated quark PDFs, $u(x_1, Q)u(x_2, Q)$, etc. From this discussion, we conclude that the $u\bar{d}$ and $d\overline{u}$ interference contributions cancel when integrated over the signal region. The largest surviving interference is due to the uu, ud, and dd terms. As a result the interference strongly affects dependence on u and d quark PDFs, but only marginally on the $\overline{d}$ antiquark PDF.

C. Parton flavor composition of $d\sigma/dy$

In Fig. 4(a), we show partial contributions to the $\mathcal{O}\left(\alpha_{EW}^2\right)$ cross sections $d\sigma/dy$ at $70 < Q < 90$ GeV involving only W^+ and W^- contributions in all channels. In this figure, we identify contributions proportional to $u(x_1)$, $d(x_1)$, $\overline{u}(x_1)$, and $\bar{d}(x_1)$. The pure $W^\pm$ contribution is dominated by the resonant terms. Hence the curves in Fig. 4(a) closely follow the rapidity dependence suggested by Eqs. (6) and (7). Only one term [proportional to $u(x)$ or $d(x)$ at $x \to 1$] survives on the right-hand sides of these equations when y approaches its kinematical limits, $y \to \pm \ln(Q/\sqrt{s})$.

The cross section supplied by W^- contributions constitutes about 1/3 of that from W^+ contributions. Consequently, the combined $W^\pm$ cross section is dominated by $u(x_1)$ and $\bar{d}(x_1)$ contributions at large positive and negative y, as in resonant W^+ production.

Figure 4(b) shows the quark flavor decomposition for the electroweak+interference $\mathcal{O}(\alpha_{EW}^2 + \alpha_s\alpha_{EW})$ cross section. In this case, the combined $u(x_1)$ contribution is roughly equal to the sum of the W^+ contribution in Fig. 4(a) and uu, ud interference contribution (symmetric with respect to $y = 0$). The combined $d(x_1)$ contribution is similarly made of the W^- and dd, du interference contributions. Both $\overline{u}(x_1)$ and $\overline{d}(x_1)$ contributions remain dominated by the resonant $W^\pm$ terms, as the interference involving sea quarks is quite small. The essential conclusion to be drawn is that the combined electroweak+interference cross section largely preserves the PDF dependence of the resonant W^+ production, notably, the sensitivity to $u(x_1, Q)$ ($\overline{d}(x_1, Q)$) at the forward (backward) y values.

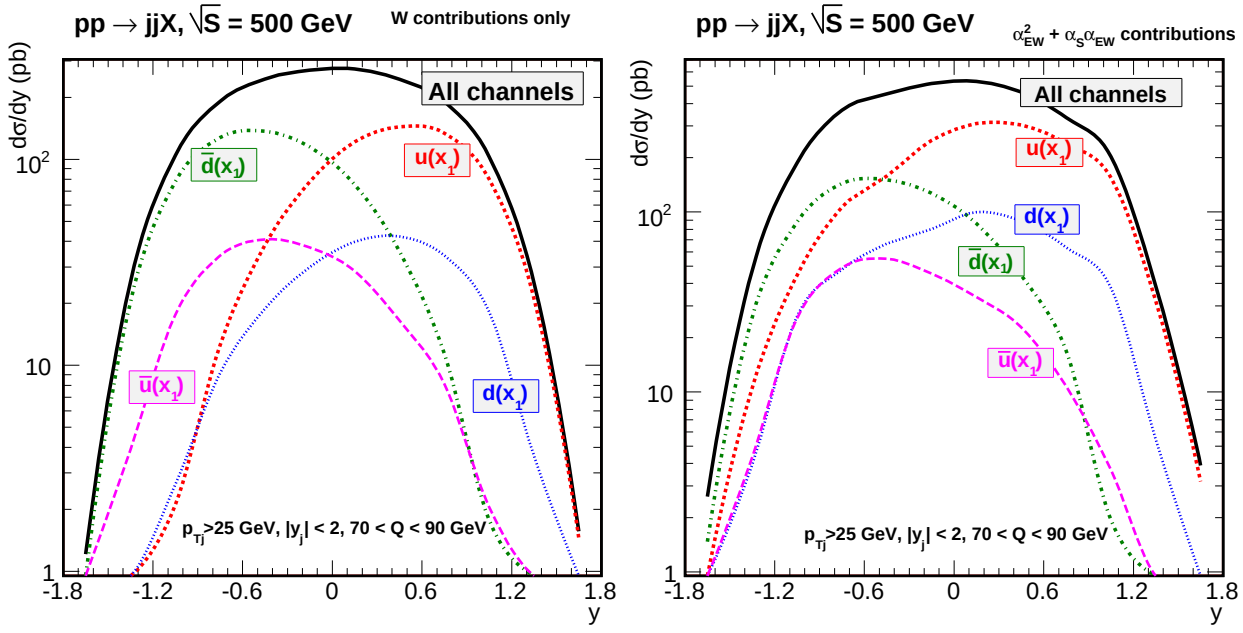

(a) (b)

Figure 4: Quark flavor composition of the unpolarized cross section $d\sigma/dy$: (a) $W(\alpha_{EW}^2)$ cross section only; (b) full electroweak+interference $\mathcal{O}(\alpha_{EW}^2 + \alpha_s\alpha_{EW})$ cross section

III. THE SINGLE-SPIN ASYMMETRY

In Fig. 5 we present the single-spin asymmetry $A_L(y)$, evaluated as a function of rapidity for two sets of DNS'2005 leading-order polarized PDFs and MRST'2002 NLO unpolarized PDFs. The statistical uncertainty δA_L in the measurement of the asymmetry is evaluated as [12]

$$\delta A_L = \sqrt{\frac{1}{\mathcal{L}\sigma}\left(\frac{1}{P_{beam}^2} - A_L^2\right)} \tag{10}$$

for the integrated luminosity $\mathcal{L} = 160$ pb^{-1} and proton beam polarization $P_{beam} = 0.7$.

The asymmetry A_L and its projected statistical uncertainty can be determined in two ways. In the first (most straightforward) method, the spin-averaged cross section is taken to be the full $\mathcal{O}\left(\alpha_S^2 + \alpha_s\alpha_{EW} + \alpha_{EW}^2\right)$ cross section. The resulting rapidity (y) dependence of A_L in the signal region $70 < Q < 90$ GeV is shown in Fig. 5(a). The value of A_L is generally small, and the statistical uncertainties (evaluated based on the total number of events for both beam polarizations in each bin) do not allow discrimination between the sets of polarized PDFs shown.

In the second method, we set the unpolarized cross section equal to the $\mathcal{O}\left(\alpha_s\alpha_{EW} + \alpha_{EW}^2\right)$ cross section both in the denominator of A_L and δA_L. This procedure is roughly equivalent to the measurement of A_L in which the background cross section (dominated by the $\mathcal{O}(\alpha_s^2)$ term) is measured precisely in the side bands ($Q < 70$ GeV and $Q > 90$ GeV), extrapolated into the signal region ($70 < Q < 90$ GeV), and subtracted from the measured unpolarized rate. Using this approximate side-band subtraction technique in Fig. 5(b), we see that the predicted magnitude of A_L is increased substantially, and different parametrizations of the

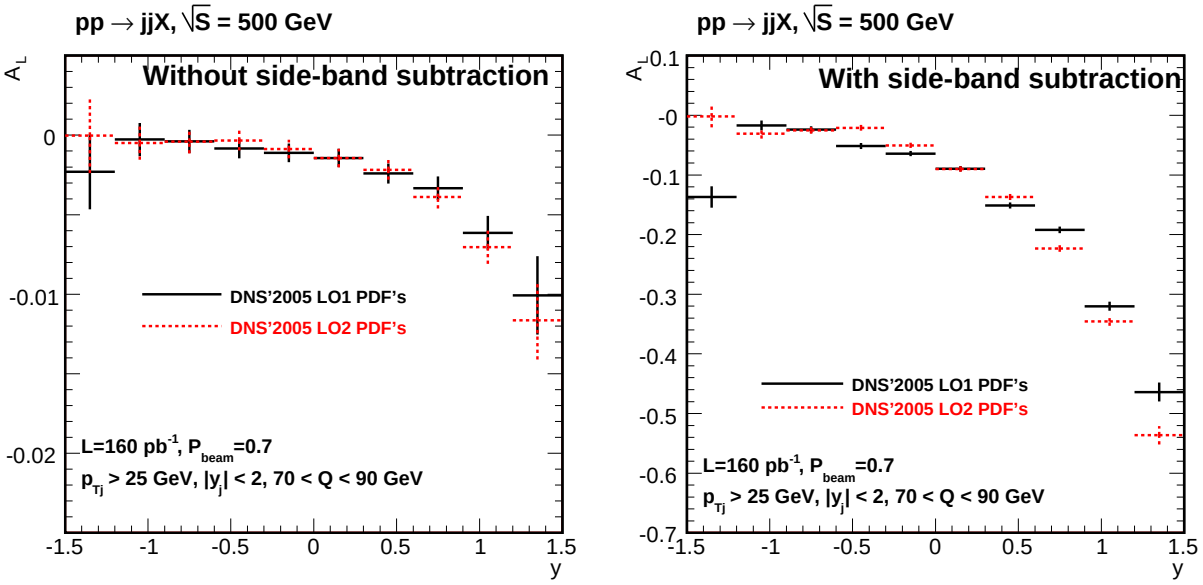

Figure 5: Parity-violating asymmetry A_L in the dijet mass interval $70 < Q < 90$ GeV without and with side-band subtraction of the parity-conserving QCD background, plotted for two sets of leading-order DNS'2005 polarized PDFs.

polarized PDFs can be discriminated, given the projected statistical uncertainties.

The asymmetry A_L includes both the W^+ and W^- contributions, as a result of summation over all jet charges. At large positive y, A_L approximately follows $-\Delta u(x)/u(x)$ at large x, expected to satisfy $\Delta u(x)/u(x) \to 1$ in the $x \to 1$ limit. At large negative y, A_L mostly reflects the behavior of sea quark PDFs at $x \to 0.02$, notably of $\Delta\overline{d}(x)/\overline{d}(x)$.

We now examine the region of negative y in greater detail in order to gauge the sensitivity of A_L to variations in the polarized PDFs within the limits tolerated by current parametrizations. We plot the values of A_L obtained after side-band subtraction for the DNS'05 NLO PDF sets with varied first moments of $\Delta u(x)$, $\Delta d(x)$, $\Delta\overline{u}(x)$, and $\Delta\overline{d}(x)$. The results are shown in Fig. 6. When $y < -1$, A_L is clearly sensitive to the variation in the first moment of $\Delta\overline{d}$ and, to a smaller degree, of $\Delta\overline{u}$. It is nearly insensitive to the variations in Δu and Δd. This result suggests that the measurement of A_L will constrain $\Delta\overline{d}(x)$, given the projected statistical uncertainties.

We remark that the pronounced sensitivity of A_L to $-\Delta u(x)/u(x)$ and $\Delta\overline{d}(x)/\overline{d}(x)$ arises because of the dominance of the W^+ contribution to parity-violating dijet production, nearly independently of the PDF set chosen. Equations (1, 6-9) state that the resonant parity-violating part of A_L behaves at large $|y|$ approximately as

$$\lim_{y\to -\ln\left(M_W/\sqrt{s}\right)} A_L(y) \approx -\frac{\frac{\Delta u(x_1)}{u(x_1)} + \frac{\Delta d(x_1)}{d(x_1)} r(x_1,x_2)}{1 + r(x_1,x_2)}, \tag{11}$$

and

$$\lim_{y\to \ln\left(M_W/\sqrt{s}\right)} A_L(y) \approx \frac{\frac{\Delta\overline{d}(x_1)}{\overline{d}(x_1)} + \frac{\Delta\overline{u}(x_1)}{\overline{u}(x_1)} r(x_2,x_1)}{1 + r(x_2,x_1)}, \tag{12}$$

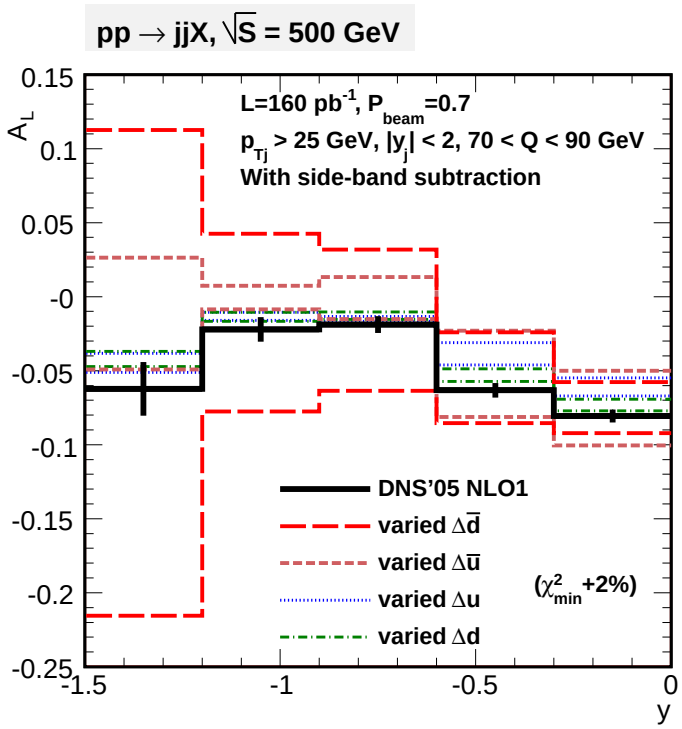

Figure 6: The asymmetry A_L for backward production of jet pairs ($y < 0$), computed for DNS'2005 NLO polarized PDFs [25] after side-band subtraction. The black solid curve corresponds to the best-fit PDF set 1. The pairs of other curves correspond to the maximal and minimal values of A_L obtained if the first moment $\Delta q \equiv \int_0^1 dx \Delta q(x, Q = 3.16 \text{ GeV})$ deviates from its best-fit value by an amount corresponding to $\chi^2 = 1.02\chi^2_{min}$, where χ^2_{min} is the minimum of the log-likelihood function χ^2 in the fit. We show A_L for varied $\Delta\overline{d}$ (red long dashes); varied $\Delta\bar{u}$ (brown short dashes); varied Δu (blue dots); and varied Δd (green dot-dashes). At large negative rapidities, the most pronounced variations in A_L are due to the variation of $\Delta\bar{d}$.

where

$$r(x_1, x_2) \equiv \frac{d(x_1)}{u(x_1)} \frac{\bar{u}(x_2)}{\bar{d}(x_2)}. \tag{13}$$

The factor r is small (of order 1/3) in both limits, as a consequence of the smallness of the $d(x)/u(x)$ ratio at $x \to 1$ (see, e.g., Figs. 3-6 in Ref. [29]). Unless $\Delta u(x_1)/u(x_1)$ is much smaller than $\Delta d(x_1)/d(x_1)$ in absolute magnitude, it dominates the numerator of $A_L(y)$ in Eq. (11). Similarly, $\Delta\bar{d}(x_1)/\overline{d}(x_1)$ dominates the numerator of Eq. (12), unless it is much smaller than $\Delta\overline{u}(x_1)/\overline{u}(x_1)$ in absolute magnitude.

In the lepton decay mode, the positron from a W^+ decay tends to scatter into the central rapidity region, hence smearing the x dependence of the underlying $\overline{d}$ parton distribution [14, 30]. In jet production, the smearing does not occur as a result of the direct measurement of the rapidity y of the jet pair.

Observation of A_L in the jet pair mode, after the background subtraction, appears to guarantee a large asymmetry associated with $\Delta u(x)$ at $x \to 1$ for forward jet pair rapidities and to test $\Delta\overline{d}(x)$ in the region of negative jet pair rapidities.

IV. CONCLUSIONS AND DISCUSSION

Data on W production obtained from longitudinally polarized proton-proton scattering at RHIC can be used to extract spin-dependent quark and antiquark parton distributions $\Delta q_i(x, M_W)$ and $\Delta \bar{q}_i(x, M_W)$, providing information complementary to that obtained from polarized deep-inelastic lepton scattering. The longitudinal spin asymmetry $A_L(y)$ of the rapidity (y) dependence of W production is particularly sensitive to the spin-dependent quark PDFs. In this paper, we examine the prospects for definitive measurements of $A_L(y)$ when the W boson is detected at RHIC in its hadronic decay mode, $W \to 2$ jets, at the collision energy $\sqrt{s} = 500$ GeV.

To take advantage of the increase in the event rate and, in principle, of the direct measurement of y offered by the hadronic decay mode, one must first address the challenges of the large parity-conserving background from QCD and electromagnetic production of jets in the vicinity of the W signal. In Sec. II of this paper, we report our tree-level computation of the amplitudes for all electroweak and strong interactions processes that lead to a pair of jets in proton-proton scattering. We treat carefully all effects of interference among the subprocesses. As shown in Fig. 1, the backgrounds in unpolarized scattering appear admittedly daunting. Most of this background is due to subprocesses with emission of one or two final-state gluons, as shown in Fig. 2. Nevertheless, even at the unpolarized level, an experimental side-band subtraction procedure could be used to reach acceptable sensitivity to events containing two final-state quarks from electroweak scattering or QCD-electroweak interference. With this procedure in place, the unpolarized event rate is dominated by processes involving the u quark PDF in the forward region of the dijet y, and by processes involving the $\bar{d}$ antiquark PDF in the backward region of y, even without separation of dijets from W^+ and W^- production [cf. Fig. 4(b)].

Turning to the longitudinally polarized case, we remark first that the largest QCD and electromagnetic backgrounds cancel in the parity-violating numerator $\sigma(p^{\rightarrow}p) - \sigma(p^{\leftarrow}p)$ of $A_L(y)$. This means that the desired sensitivity of $A_L(y)$ to $\Delta u(x, M_W)$ and $\Delta \overline{d}(x, M_W)$ is mostly preserved. The magnitude of $A_L(y)$ can be enhanced by applying the above subtraction procedure to the spin-averaged denominator $\sigma(p^{\rightarrow}p) + \sigma(p^{\leftarrow}p)$ of $A_L(y)$. The strong and electromagnetic backgrounds may be measured in the dijet invariant mass distribution in side-band regions next to the W signal location. An appropriate extrapolation and subtraction of the backgrounds may then be performed when defining the denominator of $A_L(y)$.

Our quantitative predictions for the asymmetry are presented in Figs. 5 and 6. In Fig. 5, we demonstrate that, once the side-band subtraction technique is employed, the predicted magnitude of A_L is sufficiently large, when compared to the expected uncertainties. The data on $A_L(y)$ would thus be a very valuable component of a global analysis leading to definitive longitudinally polarized PDFs.

At large positive y, A_L approximately tracks $-\Delta u(x)/u(x)$ at large x, commonly assumed to satisfy $\Delta u(x)/u(x) \to 1$ at $x \to 1$. We find that A_L can drop as low as -0.5 at $y = 1.2-1.5$ (Fig. 5(b)). The statistical error in this range of y is still small enough to allow a meaningful measurement.

At large negative y, A_L reflects the behavior of the sea quark density $\Delta \overline{d}(x)/\overline{d}(x)$. One way to estimate the power of discrimination is to compute the changes in the predicted $A_L(y)$ that result from varying the polarized parton densities within the bands of tolerance of current parametrizations. As shown in Fig. 6, the most pronounced predicted variations

in the backward rapidity region result from changes in $\Delta\bar{d}$.

In an effort to increase the magnitude of $A_L(y)$, several techniques may prove to be helpful. Selection of events at central $\Delta y = |y_1 - y_2|$ (or central $\cos\theta_*$ in the dijet rest frame) helps to suppress the gluon-dominated QCD background, as follows from Figs. 1(c) and 2(b).

One may consider selecting jets containing a final-state charmed particle [24]. In this case, the QCD background is reduced much more than the W signal rate by excluding many sources of light-flavored jets. Using realistic efficiencies for charm detection, we cannot conclude that the charm tag clearly improves the expected significance of the measurements of $A_L(y)$. An alternative approach could involve a tag on a leading charged particle in the jet (e.g., a charged pion carrying at least a third of the total jet energy) to emphasize contributions of the quark-initiated jets over gluon-initiated jets. As with the charm tags, the reduction in the background over signal in this case must be balanced against the substantial suppression in the total event rate. We therefore defer our conclusion about the feasibility of charm and leading-particle tags until a more detailed study.

The analysis reported here uses hard-scattering cross sections computed at the lowest order in perturbation theory. Next-to-leading order (NLO) contributions in QCD increase the predicted rates for hadronic jet production [31, 32] and are essential for reducing large scale dependence of the lowest-order cross section. This increase means that the backgrounds in the denominator of $A_L(y)$ can be larger than our estimates. On the other hand, as shown by Moretti *et al.* [33], comparably large enhancements are predicted in the single spin polarized cross sections at RHIC, meaning naively that the predicted magnitude of $A_L(y)$ could remain largely unaffected. A quantitative statement about the ultimate effects of NLO terms on $A_L(y)$ would require a consistent treatment of NLO contributions to all contributing processes, in both the unpolarized and polarized cases, as well as consistent application of kinematic selections that we find advantageous. We leave this task for future work, but we note here that comparably large enhancements of both the polarized and unpolarized rates would lead to a *decrease* in the projected statistical uncertainty δA_L, Eq. (10), since δA_L is proportional to $1/\sqrt{N}$, where N is the number of events observed.

Our essential conclusion is that an experimental study of high-p_T jet pair production at RHIC appears to offer a promising way to make definitive measurements of the longitudinal spin asymmetry $A_L(y)$.

Acknowledgments

The motivation for this work and preliminary estimates were discussed by P. M. N. at RHIC Spin Workshops at Brookhaven National Laboratory in October, 2005 and April 2007. We are grateful to the organizers of these workshops for the stimulating environment. P. M. N. is particularly grateful to S. Arnold, A. Metz, and W. Vogelsang for enlightening discussions of the presented topics.

E. L. B. is supported by the U. S. Department of Energy under Contract No. DE-AC02-06CH11357. P. M. N. is partly supported by the U.S. Department of Energy under grant DE-FG02-04ER41299, and by Lightner-Sams Foundation. The authors thank the Kavli Institute for Theoretical Physics (KITP), Santa Barbara, for hospitality during the course of some of this work. The KITP is supported by the National Science Foundation under

Grant No. NSF PHY05-51164.

---

[1] E. L. Berger, F. Halzen, C. S. Kim, and S. Willenbrock, Phys. Rev. **D40**, 83 (1989), erratum: *ibid.*, D**40**, 3789 (1989).

[2] F. Abe et al. (CDF Collaboration), Phys. Rev. Lett. **68**, 1458 (1992).

[3] F. Abe et al. (CDF Collaboration), Phys. Rev. Lett. **74**, 850 (1995), hep-ex/9501008.

[4] A. D. Martin, W. J. Stirling, and R. G. Roberts, Phys. Rev. **D47**, 867 (1993).

[5] H. L. Lai et al., Phys. Rev. **D55**, 1280 (1997), hep-ph/9606399.

[6] E. L. Berger, in Proceedings of the Symposium on Future Polarization Physics at Fermilab, Batavia, IL, June, 1988 (unpublished).

[7] C. Bourrely and J. Soffer, Phys. Lett. **B314**, 132 (1993).

[8] C. Bourrely and J. Soffer, Nucl. Phys. **B423**, 329 (1994), hep-ph/9405250.

[9] P. M. Nadolsky (1995), hep-ph/9503419.

[10] T. Gehrmann, Nucl. Phys. **B534**, 21 (1998), hep-ph/9710508.

[11] M. Gluck, A. Hartl, and E. Reya, Eur. Phys. J. **C19**, 77 (2001), hep-ph/0011300.

[12] G. Bunce, N. Saito, J. Soffer, and W. Vogelsang, Ann. Rev. Nucl. Part. Sci. **50**, 525 (2000), hep-ph/0007218.

[13] V. Barger and R. Phillips, *Collider physics* (Addison-Wesley, 1988), chap. 8.

[14] P. M. Nadolsky and C.-P. Yuan, Nucl. Phys. **B666**, 31 (2003), hep-ph/0304002.

[15] P. M. Nadolsky and C.-P. Yuan, Nucl. Phys. **B666**, 3 (2003), hep-ph/0304001.

[16] B. Kamal, Phys. Rev. **D57**, 6663 (1998), hep-ph/9710374.

[17] C. Bourrely, J. P. Guillet, and J. Soffer, Nucl. Phys. **B361**, 72 (1991).

[18] J. Pumplin, Phys. Rev. **D45**, 806 (1992).

[19] U. Baur et al. (2000), hep-ph/0005226.

[20] R. Ansari et al. (UA2 Collaboration), Phys. Lett. **B186**, 452 (1987).

[21] T. Stelzer and W. F. Long, Comput. Phys. Commun. **81**, 357 (1994), hep-ph/9401258.

[22] F. Maltoni and T. Stelzer, JHEP **02**, 027 (2003), hep-ph/0208156.

[23] J. Alwall et al., JHEP **09**, 028 (2007), arXiv:0706.2334.

[24] S. Arnold, A. Metz, and W. Vogelsang (2008), arXiv:0807.3688.

[25] D. de Florian, G. A. Navarro, and R. Sassot, Phys. Rev. **D71**, 094018 (2005), hep-ph/0504155.

[26] H. Murayama, I. Watanabe, and K. Hagiwara (1992), preprint KEK-91-11.

[27] A. D. Martin, R. G. Roberts, W. J. Stirling, and R. S. Thorne, Eur. Phys. J. **C28**, 455 (2003), hep-ph/0211080.

[28] J. W. Harris (STAR Collaboration), Nucl. Phys. **A566**, 277c (1994).

[29] J. F. Owens et al., Phys. Rev. **D75**, 054030 (2007), hep-ph/0702159.

[30] G. Bunce et al. (2008), RHIC Spin Physics Plan, http://spin.riken.bnl.gov/rsc/, Appendix D.

[31] S. D. Ellis and D. E. Soper, Phys. Rev. Lett. **74**, 5182 (1995), hep-ph/9412342.

[32] W. T. Giele, E. W. N. Glover, and D. A. Kosower, Phys. Rev. **D52**, 1486 (1995), hep-ph/9412338.

[33] S. Moretti, M. R. Nolten, and D. A. Ross, Phys. Lett. **B643**, 86 (2006), hep-ph/0509254.